universe

MDPI

Article

The Gaussian-Drude Lens: A Dusty Plasma Model Applicable to Observations Across the Electromagnetic Spectrum

Adam Rogers [1,2]

[1] Department of Physics and Astronomy, Brandon University, Brandon, MB R7A 6A9, Canada; rogersa@brandonu.ca
[2] Department of Physics and Astronomy, University of Manitoba, Winnipeg, MB R3T 2N2, Canada

Abstract: When radiation from a background source passes through a cloud of cold plasma, diverging lensing occurs if the source and observer are well-aligned. Unlike gravitational lensing, plasma lensing is dispersive, increasing in strength with wavelength. The Drude model is a generalization of cold plasma, including absorbing dielectric dust described by a complex index of refraction. The Drude lens is only dispersive for wavelengths shorter than the dust characteristic scale ($\lambda \ll \lambda_d$). At sufficient photon energy, the dust particles act like refractive clouds. For longer wavelengths $\lambda \gg \lambda_d$, the optical properties of the Drude lens are constant, unique behavior compared to the predictions of the cold plasma lens. Thus, cold plasma lenses can be distinguished from Drude lenses using multi-band observations. The Drude medium extends the applicability of all previous tools, from gravitational and plasma lensing, to describe scattering phenomena in the X-ray regime.

Keywords: gravitational lensing; compact objects; plasma; dust

check for updates

Academic Editors: Francesco De Paolis, Alexander F. Zakharov and Luka Č. Popović

Received: 1 December 2024
Revised: 17 January 2025
Accepted: 20 January 2025
Published: 26 January 2025

Citation: Rogers, A. The Gaussian-Drude Lens: A Dusty Plasma Model Applicable to Observations Across the Electromagnetic Spectrum. *Universe* **2025**, *11*, 40. https://doi.org/10.3390/universe11020040

1. Introduction

Gravitational lensing is a well-known astronomical phenomenon that affects our view of the distant Universe [1]. This type of lensing occurs when light rays pass through the curved spacetime produced by a massive object [2]. It produces images on a variety of scales [3] and provides awe-inspiring views of distant cosmic vistas as if seen in the distorted glass of a funhouse mirror [4].

While gravitational lensing is arguably the most well-known optical phenomenon that distorts our view of the Universe, there are many physical media that are relevant to the paths along which radiation arrives at our instruments. For example, plasma is the most common state of matter in the Universe, constituting the ionized material between the stars, the interstellar medium (ISM).

Plasma lensing occurs independently of gravitational lensing. For example, extreme scattering events (ESEs) are believed to be caused by small, highly over-pressured structures on sub-AU scales [5,6]. These structures produce optical effects when they obscure bright background radio sources. Unlike the strictly converging behavior of gravitational lenses, plasma is both diverging and dispersive (chromatic). There are many studies that combine both gravitational and plasma lensing effects [1,7], but these are often complicated by the need for extremely low-frequency observations [8].

In addition to plasma, dust is also ubiquitous throughout the cosmos, comprising about 1% of the ISM. There is a strong connection between X-ray scattering and the properties of dust grains that affect them [9] at all distances, from interstellar [10,11] to intergalactic

scales [12]. Examples of dust rings from bright X-ray transients are known from galactic sources [13–17], as well as from the afterglow of long-duration gamma-ray bursts (GRBs; [18]).

Achromatic gravitational lenses, as well as optical events from dispersive astrophysical processes across the electromagnetic spectrum from the dust scattering of gamma-ray bursts (GRBs; [19]) to the propagation of fast radio bursts (FRBs; [20]) can be modeled using a common framework which yields the usual lensing information such as magnification and image time delays, along with the absorption due to intervening material along the line of sight.

Wagner and Er [21] compared the formalism for gravitational and plasma lensing. Our current work now extends the applicability of the gravitational lens thin-lens framework to X-ray dust-scattering phenomena using the Drude medium. The Drude model includes absorption, which produces the correct energy dependence of the optical depth in the high energy range, where the refractive effects are minimal [22]. Despite the scattering nature of the X-ray phenomena, the lensing formalism reproduces all related formulae from the X-ray literature. For X-rays the dust particles are like small, refractive clouds, determined by their dielectric properties. In the X-ray regime, we derive the properties of dust scattering used in the literature.

We consider a spherically symmetric semi-transparent lens analogous to our previous work in gravitational lensing with an absorbing medium [22]. We wish to specialize these earlier results to the case when a compact object is not present and consider only a lossy medium arranged in a spherically symmetric cloud that acts as a dispersive, diverging refractive lens in the interstellar medium (ISM). This model extends the Gaussian lens model originated by Clegg, Fey & Lazio (CFL; [5]), which has been used extensively in the literature to model the refractive objects responsible for extreme scattering events (ESEs) in background radio sources.

Consider a complex index of refraction,

$$n^2 = 1 + \chi_R + i\chi_I \tag{1}$$

where i is the unit imaginary number, χ_R and χ_I are the real and imaginary susceptibility. We seek to describe electromagnetic radiation passing through a spherical region of Drude medium, an absorbing dielectric that can be thought of as a model for the permittivity of a "dusty plasma".

$$n^2(r) = 1 - \frac{\omega_p^2(r)}{\omega^2 + \omega_d^2} + i\Big(\frac{\omega_d}{\omega}\Big)\frac{\omega_p^2(r)}{\omega^2 + \omega_d^2}, \tag{2}$$

using the frequency of the radiation ω and where $\omega_d = 1/\tau_d$ is the dust collision frequency [23–27]. The plasma frequency is

$$\omega_p^2(r) = 4\pi\frac{q^2 n_p(r)}{m} \tag{3}$$

where $n_p(r)$ is the plasma density. The classical electron radius is

$$r_e = \frac{q^2}{mc^2} \tag{4}$$

in cgs units, with the charge and mass of the electron q and m, respectively. In the limit where interactions between radiation and absorbing dust are infrequent, the Drude model reproduces cold plasma behavior [28–30]. On the other hand, when radiation and dust interact, absorption often dominates over refraction, producing low-angle deflection similar to the behavior of X-ray scattering due to interaction with dust [31,32]. For intermediate val-

ues of λ_d, the Drude model produces unique and novel results that include both refraction and absorption.

The purpose of this study is two-fold. First, we wish to examine the implied grain size for modest amounts of absorption using the set of extreme model configurations responsible for ESEs since they are a set of observations that have been modeled with Gaussian Plasma lenses [5]. Since the Drude medium is a generalization of the cold plasma index of refraction, it is reasonable to evaluate the physical plausibility of absorption under extreme circumstances. We restrict our study to absorption in the 1% and 5% range, chosen arbitrarily.

In the weak-field regime where microlensing-type behavior occurs, the Drude medium attains a constant, asymptotic value that depends on the parameters of the dust present. Rather than assume a constant grain size, we will fit each observation individually. This allows us to determine if absorption is at least physically plausible in a given source and what grain size is required to approximately match the published results to 1% agreement. This precision limit is chosen arbitrarily to "sufficiently" reproduce the literature results without introducing other obvious observational effects. If absorption is important, we assume that its effect has been compensated for in the lens parameter fitting and that absorption in such systems will not be too strong.

2. Theory

We first establish some basic results from the lensing literature [1,21] and then explore how those outcomes must be modified to accommodate an absorbing medium.

The gravitational lensing formalism depends on the thin-lens assumption, and the extent of the scale of the scattering body is small, which is inherited by the deflection angle and the index of refraction. Thus, generally, this approach requires the frequency of the propagating radiation to be substantially smaller than both the plasma and dust frequency scales in the problem. For this work we consider only this limited approach, though the model can be extended to wider ranges of applicability. We note this also excludes the case in which both ω and ω_d are substantially smaller than the plasma frequency ω_p scale.

Let the angular coordinates on the image plane, at a distance D_d from the observer, be defined in terms of the impact parameter of a ray $b = D_d\theta$, where θ is the angle on the observer's sky (the image plane). Following the usual gravitational lens conventions, we take the distance from the observer to the source as D_s and the distance from the lens deflector to source D_{ds}. We assume spherical symmetry for simplicity, with β the angular position of the source and θ the angular position of the resulting image. The thin-lens equation that translates from source coordinates (β) to image coordinates measured on the sky (θ) using the deflection angle $\alpha(\theta)$ is

$$\beta(\theta) = \theta - \alpha(\theta). \tag{5}$$

The projected plasma density on the lens plane is

$$N_p(\theta) = \int_{-\infty}^{+\infty} n_p(D_d\theta, z)dz. \tag{6}$$

The effective plasma lens potential [33] is

$$\psi(\theta) = \frac{D_{ds}}{D_s D_d}\frac{1}{2\pi} r_e \lambda^2 N_p(\theta) \tag{7}$$

in terms of the wavelength of radiation λ. For a given effective potential, the deflection angle [3] is

$$\alpha(\theta) = \nabla_\theta \psi(\theta) \tag{8}$$

which gives, using Equation (7),

$$\alpha(\theta) = \frac{D_{ds}}{D_s D_d} \frac{1}{2\pi} r_e \lambda^2 \nabla_\theta N_p(\theta). \tag{9}$$

A well-known identity exists [34,35] which solves the deflection angle for power-law type plasma density $n_p(r)$ [22]. However, in this work, we seek the deflection angle in terms of projected density N_p, following [5].

Absorbing media are dusty plasmas that are described by the Drude [36] index of refraction given in Equation (2). We note that the real part of the index of refraction is the cold plasma index of refraction modified by adding the collision frequency to the wave frequency. In the weak-deflection limit, it has been shown [22] the Drude medium deflection angle reproduces the cold plasma results found in the literature [28–30] provided $\omega^2 \to \omega^2 + \omega_d^2$. Given the wavelength $\lambda = 2\pi c/\omega$ and the average collision distance between photons and dust particles, $\lambda_d = 2\pi c/\omega_d$ leads to a substitution for the modified effective lens potential (Equation (7)) and modified deflection angle (Equation (9)),

$$\lambda^2 \to \left(\frac{1}{\lambda^2} + \frac{1}{\lambda_d^2} \right)^{-1} = \frac{\lambda^2 \lambda_d^2}{(\lambda^2 + \lambda_d^2)}. \tag{10}$$

We note that the first expression on the right-hand side allows for easy visual evaluation of the limit in which the mean collision distance λ_d grows large. In this case, the Drude model reproduces the cold plasma index of refraction [22,36]. The limiting behavior of the second expression on the right-hand side requires L'Hopital's rule. Let us define shorthand for the Drude effective wavelength,

$$\Lambda_D^2 = \frac{\lambda^2 \lambda_d^2}{(\lambda^2 + \lambda_d^2)}. \tag{11}$$

In terms of frequency dependence, it is Λ_D that distinguishes between cold plasma $\Lambda_{CP}^2(\lambda) = \lambda^2$ and Drude medium $\Lambda_D(\lambda, \lambda_d)$ by Equation (11). We note that the average collision distance λ_d is chosen to be constant. While the constant density of dust is an artificial feature of the model, particularly in view of the changing plasma density, it allows us to obtain an upper limit on the dust grain size for a given choice of collision scale. A more realistic and physical choice, left for future work, is to consider the variation in both plasma and dust density separately, perhaps using independent Gaussian distributions.

For completeness, the modified deflection angle is explicitly stated,

$$\alpha(\theta) = \frac{D_{ds}}{D_s D_d} \frac{1}{2\pi} r_e \Lambda_D^2 \nabla_\theta N_p(\theta) = A \nabla_\theta N_p(\theta). \tag{12}$$

with

$$A(\Lambda_D) = \frac{D_{ds}}{D_s D_d} \frac{1}{2\pi} r_e \Lambda_D^2. \tag{13}$$

This expression depends on the gradient of the projected plasma density. For a spherically symmetric lens, we expect the density to generally decrease radially from the lens center, which provides the negative sign that flips the deflection angle from converging to diverging orientation. In the limit of vanishing dust density, i.e., when the average distance between collisions between photons and dust particles becomes infinite $\lambda_d \to \infty$ Equation (12) reproduces Equation (9).

Now that we have established the deflection angle, let us turn to the time delay.

$$t(\theta) = \frac{(1+z_d)}{c}\frac{D_d D_s}{D_{ds}}\left[\frac{1}{2}(\theta-\beta)^2 - \psi(\theta)\right] \tag{14}$$

The first term in this expression is the geometric term, which is the delay due to the physical path length. The second term, which depends on the lens potential, is the gravitational term that is due to moving in a potential, called the Shapiro delay [2,3]

$$t_{Shapiro}(\theta) = -\frac{(1+z_d)}{c}\frac{D_d D_s}{D_{ds}}\psi(\theta), \tag{15}$$

where the negative sign shows that this is a delay. In plasma lensing, this extra delay is due to the charged matter distribution along the line of sight.

$$t_{Drude}(\theta) = -\frac{(1+z_d)}{c}\frac{1}{2\pi} r_e \Lambda_D^2 N_p(\theta). \tag{16}$$

This is the same in form as the plasma lens time delay [37,38], except with the wavelength λ^2 replaced by the Drude frequency function Λ_D^2.

In addition to the usual lensing properties, We now calculate the absorption profile associated with the Drude medium. As shown in [22], the optical depth is

$$\tau_{Drude} = \int_{-\infty}^{+\infty} \chi_I \frac{\omega}{c} dz \tag{17}$$

using the definition from the Drude medium, Equation (2), we find

$$\tau_{Drude}(\theta) = 4\pi c r_e \frac{\omega_d}{\omega^2 + \omega_d^2} N_p(\theta) \tag{18}$$

or, in terms of the wavelength,

$$\tau_{Drude}(\theta) = 2r_e \frac{\Lambda_D^2}{\lambda_d} N_p(\theta) = B N_p(\theta) \tag{19}$$

with

$$B(\Lambda_D) = 2r_e \frac{\Lambda_D^2}{\lambda_d} \tag{20}$$

In the limit of infinite mean collision distance, the optical depth vanishes since the cold plasma index of refraction is purely real and hence $\chi_I = 0$ for that case.

The optical properties of the Drude medium are summarized by the pair of quantities, the deflection angle (Equation (12)) and the optical depth (Equation (19)).

2.1. Implications: The Magnification of the Drude Lens

The magnification of an absorbing lens is given by a combination of the usual Jacobian determinant of the thin-lens transformation and the optical depth of the lens plane itself. The total magnification is

$$\mu_T(\theta) = \sum_{a=1}^{N} \exp(-\tau_a)|\mu_a|. \tag{21}$$

with the images indexed by the subscript a. Since the lens is spherically symmetric, the refractive magnification is comprised of two factors,

$$\mu(\theta) = \frac{\theta}{\beta}\frac{d\theta}{d\beta}. \tag{22}$$

The images have tangential magnification

$$\mu_{t,a}^{-1}(\theta_a) = \frac{\beta_a}{\theta_a} = 1 - \frac{A}{\theta_a}\frac{dN_p}{d\theta}\bigg|_{\theta=\theta_a} \tag{23}$$

and radial magnification

$$\mu_{r,a}^{-1}(\theta_a) = \frac{d\beta_a}{d\theta}\bigg|_{\theta=\theta_a} = 1 - A\frac{d^2N_p}{d\theta^2}\bigg|_{\theta=\theta_a}. \tag{24}$$

Putting these two expressions together gives the total magnification for a given image

$$\begin{aligned}\mu_{T,a}(\theta_a) = \quad & \Big[1 - \tfrac{A(\Lambda_D)}{\theta_a}\tfrac{dN_p}{d\theta}\Big|_{\theta=\theta_a} - A(\Lambda_D)\tfrac{d^2N_p}{d\theta^2}\Big|_{\theta=\theta_a} \\ & + \tfrac{A^2(\Lambda_D)}{\theta_a}\left(\tfrac{dN_p}{d\theta}\Big|_{\theta=\theta_a}\right)\left(\tfrac{d^2N_p}{d\theta^2}\Big|_{\theta=\theta_a}\right)\Big]^{-1}.\end{aligned} \tag{25}$$

with $A(\Lambda_D)$ the scaling factor given in Equation (13). However, other than the difference in frequency dependence due to $A = A(\Lambda_D)$, the critical and caustic networks of the absorbed Drude material and plasma are identical in form. Despite this apparent similarity, the presence of absorbing material further complicates the calculation of the total magnification, as the optical density

$$\tau_a = B(\Lambda_D)\, N_p\big|_{\theta=\theta_a} \tag{26}$$

alters the individual intensity of each independent image by the exponential coefficient in Equation (21).

2.2. Observational Signature of the Drude Lens

The Drude medium produces a lens magnification given by Equation (25). In this expression, all terms beyond unity are dependent on a power of the coefficient A, which is itself directly linearly proportional to $\Lambda_D^2(\lambda)$. Similarly, the lens optical depth is directly proportional to $\Lambda_D^2(\lambda)/\lambda_d$. Therefore, the effective wavelength directly controls how both of these quantities evolve across the electromagnetic spectrum.

We plot both the square of the effective wavelength $\Lambda_D^2(\lambda)$, as well as the coefficient that appears in the optical depth, $\Lambda_D^2(\lambda)/\lambda_d$, in Figure 1 as a function of wavelength. We define the dimensionless size parameter as

$$x = 2\pi\frac{a}{\lambda} = \frac{\lambda_d}{\lambda} \tag{27}$$

where a is the radius of a spherical dust grain. When $x \ll 1$, we are in the Rayleigh regime, in which the grain size is much smaller than the incident radiation. In the Rayleigh limit, the absorption cross-section for dust is much larger than the scattering cross-section, so absorption processes dominate [39].

As seen in the left-hand panel of Figure 1, the effective wavelength approaches a constant asymptotic value in the Rayleigh region when the wavelength of radiation is much greater than the characteristic wavelength of dust $\lambda \gg \lambda_d$ ($x \ll 1$). In the Rayleigh regime, the magnification and optical properties of the Drude lens lose their wavelength dependence and approach an asymptotic value. In the opposite limit, outside the Rayleigh regime, we see the effective wavelength evolve as λ^2. The optical behavior of the Drude lens is only chromatic for wavelengths below the dust characteristic scale (i.e., $\lambda < \lambda_d$ or $x > 1$). This is dramatically different than the behavior of cold plasma, shown as the dashed line in Figure 1, in which the optical properties of a plasma lens evolve with

wavelength. Therefore, the key to distinguishing these models is through multi-band observations, which would be capable of determining how the lens scale evolves with wavelength. If an estimate of the turning point of Λ_D^2 could be measured (essentially determining the wavelength after which the magnification becomes constant), this would give the characteristic dust scale and the grain radius of the dust present in the lens.

When $x \gg 1$, we are considering the low-wavelength, high-frequency part of the electromagnetic spectrum. Similar to cold plasma, when the wavelength of radiation is sufficiently small, the refractive effects of the lens become weak. This describes an optical effect similar to low-angle X-ray scattering [40]. Thus, the Drude medium extends the usual applicability of gravitational and plasma lensing formalism to describe geometric optics in the X-ray regime.

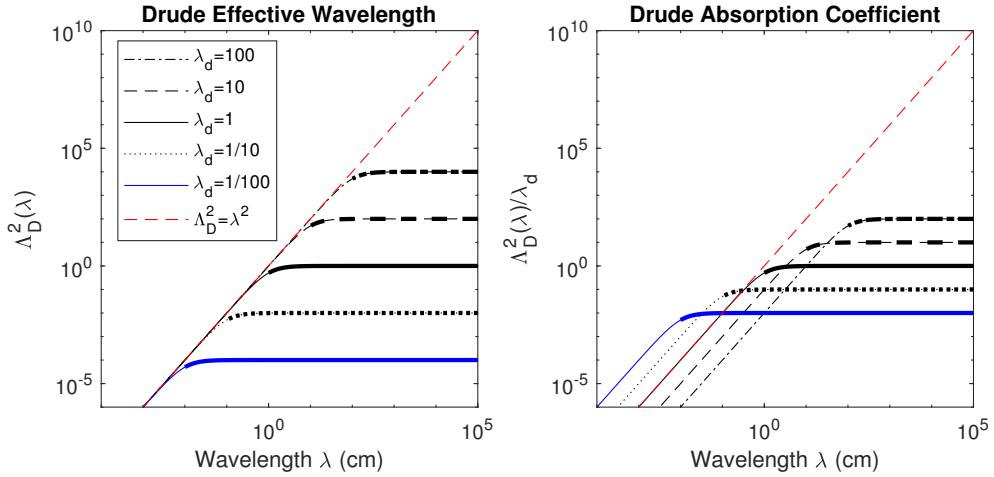

Figure 1. (**Left**): The Drude effective wavelength $\Lambda_D^2(\lambda)$ is plotted as a function of wavelength for four separate instances of the dust characteristic wavelength. The heavy curves represent the Rayleigh regime. The diagonal dashed line is the cold plasma case with $\Lambda_D^2 = \lambda^2$. (**Right**): The Drude absorption coefficient Λ_D^2/λ_d is plotted as a function of wavelength for the dust characteristic wavelength cases given in the left panel. The diagonal dashed line is $\Lambda_D^2 = \lambda^2$. Both plots are on log-log scales.

3. Radio Application: Extreme Scattering Events: The Diverging Gaussian-Drude Lens

The arguments presented so far have been totally general, depending only on the projected density N_p. These results extend the work of [22] in the absence of gravitational effects and consider the lensing properties of a projected Drude medium only.

The goal of this work is to estimate the feasibility of absorbing material in structures typically considered for plasma lensing. Arguably, the most enigmatic plasma lens structures are responsible for ESEs. Let us assume a modest absorption on the order of 1% to 5%. We are interested if such extreme lens structures predict realistic physical properties for the absorbing granular material. This feasibility study is intended as a hypothetical exercise with respect to ESEs; however, it is possible that absorbing Drude material may contribute toward some astrophysical lensing phenomenon. The lens column density depends on the projected plasma density N_p and its magnification depends on the first and second derivatives of the projected density on the plane of the sky.

Let us follow Clegg, Fey, and Lazio [5] and assume the projected density has a spherically symmetric Gaussian form,

$$N_p(\theta) = N_0 \exp\left(-\frac{\theta^2}{2\sigma^2}\right). \tag{28}$$

The CFL lens is the most widely applied model for describing ESEs [41–48]. We briefly summarize the properties of the Gaussian lens in detail. Using the definition of the characteristic radius,

$$\theta_0^2(\Lambda_D) = A(\Lambda_D)N_0 \tag{29}$$

we have

$$\alpha(\theta) = -\frac{\theta_0^2}{\sigma^2}\theta e^{-\frac{\theta^2}{2\sigma^2}} \tag{30}$$

giving the lens magnification

$$\mu_T = \left[1 + 2\frac{\theta_0^2}{\sigma^2}\left(1 - \frac{\theta^2}{2\sigma^2}\right)e^{-\frac{\theta^2}{2\sigma^2}} + \frac{\theta_0^4}{\sigma^4}\left(1 - \frac{\theta^2}{\sigma^2}\right)e^{-\frac{\theta^2}{\sigma^2}}\right]^{-1} \tag{31}$$

which agrees with the formula in [49]; (Equation (51) in that paper), provided the substitution from Equation (10) is made. The optical depth is

$$\tau_{Drude}(\theta) = 2\frac{\Lambda_D^2}{\lambda_d} r_e N_0 e^{-\frac{\theta^2}{2\sigma^2}} \tag{32}$$

and leads to the extinction factor

$$C_A(\theta) = e^{-\tau_{Drude}(\theta)}, \tag{33}$$

matching the expression in [22].

Let the radial extent of the lens be a_L cm, and the projected lens number density is $N_0 = a_L n_e$ cm^{-2}. The scattering time $T_d = a_d/c$ depends on the radius of a dust grain a_d along with the speed of light. The dust collision frequency is then $\omega_d = 1/T_d$, and gives $\lambda_d = 2\pi a_d$. This leads to the collision wavelength and allows the calculation of Λ_D, lens optical depth, deflection angle, and magnification.

While it is most likely that plasma is sufficient to describe the ESE phenomena, the Drude medium shows that a small amount of absorption may still be physically accommodated even by the over-dense structures typically associated with ESEs. The lens parameters of the ESEs previously modeled in the literature are given in Table 1, summarizing the results of [6]. We use the Gaussian lens parameters from the modeled systems to evaluate the optical depth for each system at the lens width $\theta_{crit} = \sigma$ on the lens plane.

Table 1. For each source, the estimated lens radius is R, the number density n_e, projected density N_0, and a_d is the dust grain radius in nm. Two grain radii are provided, the first of which is given for 1% and 5% absorption factors, respectively. The assumed radiation frequency used to generate table values was 1 GHz. References for ESE observations: 1 and 2: [5], 3: [42], 4: [43], 5: [44], 6 and 7: [45], 8: [46], 9: [47], 10 and 11: [48].

	Source	R (AU)	n_e (cm^{-3})	N_0 (cm^{-2})	a_d (nm, 1%)	a_d (nm, 5%)
1	0954+658	0.4	1*e*5	6*e*17	0.078	0.399
2	1741-038	0.065	300	3*e*14	160.408	818.665
3	2023+335	0.4	4*e*4	2.4*e*17	0.196	0.998
4	PKS 1939-315	0.7	1*e*3	1*e*16	4.469	22.806
5	PSR J1643-1224	56	130	1*e*17	0.859	4.386
6	PSR B1937+21	0.094	25	3*e*13	1331.046	6793.177
7	PSR B1937+21	0.05	220	2*e*14	284.360	1451.270
8	PSR B1937+21	0.6	200	2*e*15	26.066	133.033
9	PSR B1800-21	220	1.5*e*4	5*e*19	$9.479e-4$	0.005
10	PSR J1603-7202	4.9	3.4	2*e*14	187.753	958.221
11	PSR J1017-7156	13.9	3.7	8*e*14	60.820	310.402

Table 1 collects data on the observed properties of ESEs. The estimated radius R, number density n_e, and projected density N_0, as well as an estimate of the grain size a_d required for a 1% intensity drop from the literature model, as well as the grain size required for a corresponding 5% intensity drop.

4. X-Ray Application: Rings from Echoes and Haloes: The Converging Gaussian-Drude Lens

The formation of X-ray haloes requires a change in intensity in an X-ray bright source obscured by a plane of dusty material in the intervening ISM. An observer looks through the dusty plane and observes an X-ray bright ring, which demonstrates a time delay [50] based on the evolution of the source [51]. Multiple rings have been observed around a single source, with the radius of a given ring directly related to the distance of the dust plane from the observer [19]. The time delay for X-ray dust echoes is typically on the order of days. Generally, the longer a flare lasts, the thicker an X-ray ring appears in the sky. If the source is shining continuously, the entire cloud is illuminated, and instead of a ring, the presence of the dust manifests as a diffuse cloud surrounding bright X-ray sources. Such clouds are known as dust-scattering haloes and are much more common than X-ray ring echoes. However, the cloud-like form of the halo makes interpreting the exact location of the dust cloud more difficult.

The production of X-ray ring echoes can be described by several optical effects operating in tandem. First, as X-rays pass through a dusty plane, they impinge on dust particles and are deflected by scattering, which produces a ring image from a bright source. Given a deflection angle that varies with distance from the X-ray source, the required geometry is provided by the thin-lens equation, which exactly reproduces the results from the X-ray literature. The magnification corresponding to the deflection angle is simply the change in solid angle between the true source and the resulting ring image. It is a purely geometric effect given by the inverse Jacobian of the lens transformation. Second, scattering affects image formation, which spreads out the deflected light into a disk in the sky, broadening the apparent angle that the source spans in the sky. As we shall see, this optical behavior can be reproduced considering the Drude medium. In the high-frequency regime, the Drude medium essentially describes an absorbing dielectric dust. The dust grains cause both scattering and absorptive refraction within them.

4.1. The Planar-Drude Lens

X-ray dust-scattering echoes are produced by a deflection angle that depends linearly on the distance from the source [52]. The transformation from source into ring is found by considering deflection from the electron density in a disk situated on the line of sight. This deflection is caused by individual dust grains, which act like small gas clouds to X-rays. The area of a disk scales proportional to the square of the distance from the origin. The normalized density is

$$N_p(\theta) = N_0\left(\frac{\theta^2}{2\sigma^2}\right) \tag{34}$$

with the first derivative given by

$$\frac{dN_p}{d\theta} = \frac{N_0}{\sigma^2}\theta \tag{35}$$

and second derivative

$$\frac{d^2N_p}{d\theta^2} = \frac{N_0}{\sigma^2}. \tag{36}$$

Consider the gradient of the density producing the deflection, similar to the case in refractive lensing. We find the linear deflection angle required to produce an X-ray dust-scattering halo,

$$\alpha = \frac{\theta_0^2}{\sigma^2}\theta, \tag{37}$$

using the definition $\theta_0^2 = A(\Lambda_D)N_0$. With the thin-lens equation, we obtain

$$\beta = \theta\left(1 - \frac{\theta_0^2}{\sigma^2}\right) \tag{38}$$

or, replacing $y = \theta_0^2/\sigma^2$, we find

$$\beta = \theta(1 - y). \tag{39}$$

In this case, y describes the focusing power of the lens, where the linear dimensions of a source are increased by a factor $(1-y)^{-1}$, producing a ring by symmetry. Many studies, for example [51], begin by taking Equation (39) as given.

The magnification for the planar-Drude lens is a constant, with the image coordinates dropping out,

$$\mu_T = (1-y)^{-2} = \left(1 - 2y + y^2\right)^{-1}. \tag{40}$$

This amplification occurs because the observer receives more flux than they would if the lens were not present. This occurs for X-ray echoes because of the dust-scattering X-rays toward an observer that would ordinarily not be detectable.

X-ray rings are sensitive to changes in source brightness, displaying delays between direct and scattered components. Therefore, to connect these lens models to observations, we must calculate the time delay due to the geometric path length from scattering. Let us return once again to the lensing formalism. In the X-ray regime, the wavelength of radiation is small $x \gg 1$, and the refractive portion of the time delay, t_{Drude} (Equation (16)) vanishes. Moreover, by assuming the ring angle is large compared to the source, the time delay (Equation (14)) becomes

$$t(\theta) = \frac{(1+z_d)}{c}\frac{D_d D_s}{D_{ds}}\frac{\theta^2}{2}. \tag{41}$$

This is the usual time delay associated with dust-scattering haloes [51]. To connect with the usual notation, we will assume Euclidean distances and place the deflector at some position y from the source. This is the same parameter defined by the ratio of characteristic length θ_0^2 to Gaussian width σ^2. We will assume all distances to be Euclidean, in terms of the distance to the source D_s. Suppose that the distance to the lens (deflector) is $D_d = yD_s$ and the distance between deflector and source is $D_{ds} = (1-y)D_s$. The time delay is then

$$t(\theta) = \frac{(1+z_d)}{c}\frac{yD_s}{(1-y)}\frac{\theta^2}{2}. \tag{42}$$

which is the usual expression in the X-ray literature [50,51]. As noted by [53], this time delay is derived in the literature using the conventional methods of gravitational lensing [54]. So far, the lensing description given here identically matches the standard approach used in the literature regarding studies of X-ray haloes.

The corresponding optical depth from the Drude plane is

$$\tau_{Drude}(\theta) = BN_0\left(\frac{\theta^2}{2\sigma^2}\right). \tag{43}$$

We will return to this expression in the next section.

In this work, we have made use of the Drude form for dielectric dust. This is an effective approach in that the dust is assumed to be non-conducting. Rather than dielectric dust, conducting dust is written in terms of the optical conductivity as

$$\chi_I = \varepsilon_I = \frac{\sigma_c}{\omega} \tag{44}$$

where non-conducting dust has $\sigma_c = 0$. It has been shown [11] that the total cross-section for scattering is

$$\sigma_{scat} = 2\pi a^2\left(\frac{2\pi a}{\lambda}\right)|n-1|^2 \tag{45}$$

and the total cross-section for extinction is

$$\sigma_{ext} = \frac{8\pi}{3}a^2\left(\frac{2\pi a}{\lambda}\right)\mathrm{Im}(n-1). \tag{46}$$

Using Equation (44) in place of the Drude dielectric expression reproduces Hayakawa's results [11]. Figures 2 and 3 show the effect of scattering in the thin lens geometry.

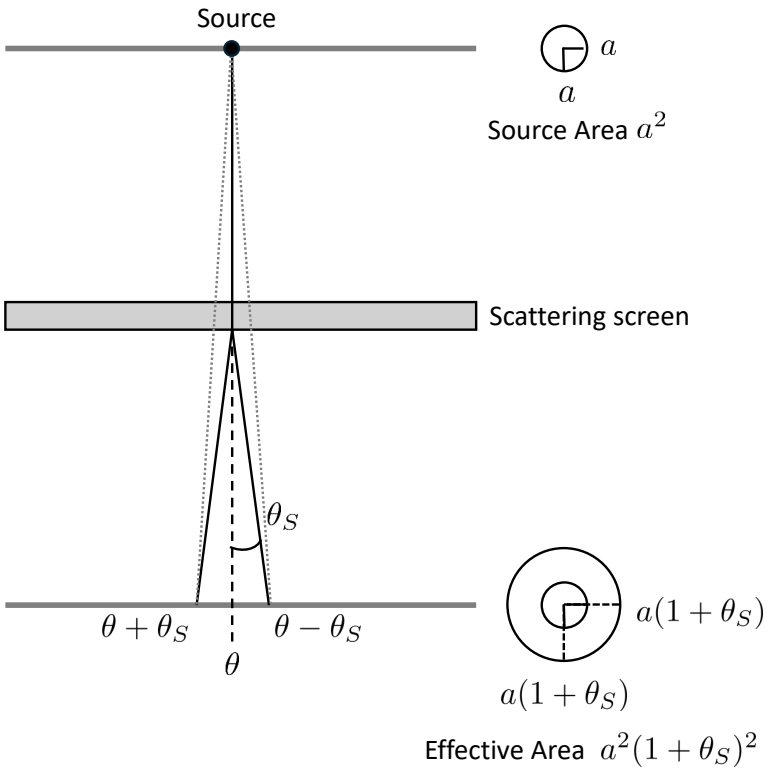

Figure 2. An example of scattering. The source is seen through a scattering screen, which produces a scatter-broadened image. The apparent dimensions of the source are symmetrically stretched by a factor of $(1+\theta_S)$.

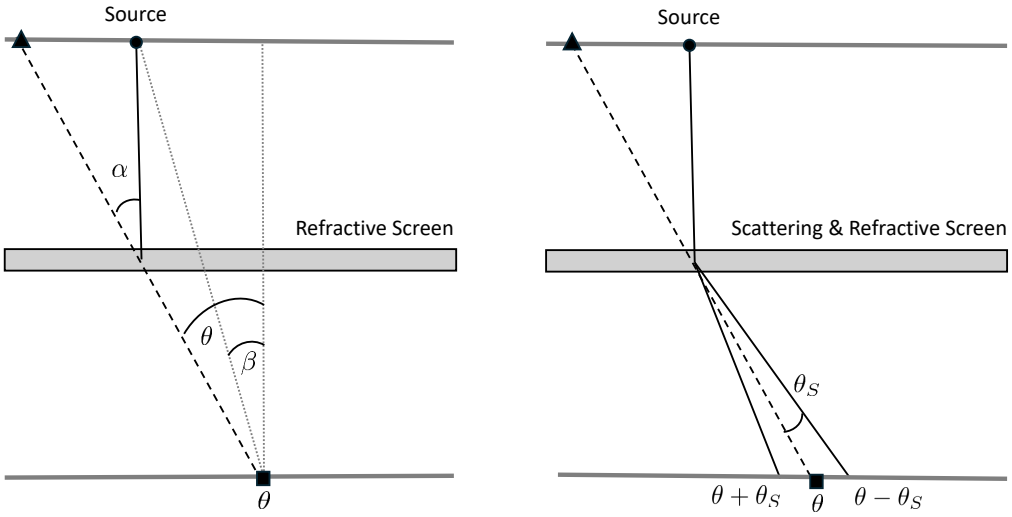

Figure 3. Imaging examples for (**Left**), the usual lensing geometry in the case of a refractive screen, and (**Right**), including both refraction and scattering. Similar to Figure 2, scattering broadens the apparent dimensions of the source.

4.2. The Converging Gaussian-Drude Lens

A similar optical effect can be achieved by considering an under-dense Gaussian-Drude lens, which behaves like a converging lens [55]. The shape of a Gaussian and the quadratic area of the uniform disk closely approximate one another near the line of sight.

To generate converging lens behavior, we begin with a Gaussian-shaped depression in an otherwise uniform background,

$$N_p(\theta) = N_0\left(1 - e^{-\frac{\theta^2}{2\sigma^2}}\right). \tag{47}$$

With the definitions of the deflection angle and magnification from Equation (12) and (25), respectively, we find

$$\alpha(\theta) = \frac{\theta_0^2}{\sigma^2}\theta e^{\frac{\theta^2}{2\sigma^2}} \tag{48}$$

and

$$\mu_T = \left[1 - 2\frac{\theta_0^2}{\sigma^2}\left(1 - \frac{\theta^2}{2\sigma^2}\right)e^{-\frac{\theta^2}{2\sigma^2}} + \frac{\theta_0^4}{\sigma^4}\left(1 - \frac{\theta^2}{\sigma^2}\right)e^{-\frac{\theta^2}{\sigma^2}}\right]^{-1} \tag{49}$$

Compared to Equation (31), we see the second term in the magnification has the sign reversed from the diverging case. Using the definition of y, we can rewrite this expression to be more similar to the planar case,

$$\mu_T = \left(1 - 2y + y^2 + y\frac{\theta^2}{\sigma^2}e^{-\frac{\theta^2}{2\sigma^2}} - y^2\frac{\theta^2}{\sigma^2}e^{-\frac{\theta^2}{\sigma^2}}\right)^{-1} \tag{50}$$

The extra terms introduce position-dependence to the magnification, which is no longer purely constant. The magnification of the planar lens Equation (40) is contained in the constant terms.

The optical depth from the Gaussian-Drude lens is

$$\tau_{Drude}(\theta) = BN_0\left(1 - e^{-\frac{\theta^2}{2\sigma^2}}\right). \tag{51}$$

Taylor expanding the exponential in the case of small θ, we recover the optical depth of the planar-Drude lens.

5. Conclusions

If absorbing material is present within a lens but not accounted for within the model used to describe it, the fitting procedure will bias the resulting parameter estimates. Our approach is to estimate the dust grain size necessary for a 1% and 5% drop in intensity at the specific location $\theta_c = \sigma$ for the model parameters given in the literature. Dust in the ISM is comprised of amorphous carbon and silicon, and the radii generally range from nm to µm scales [56]. We estimate grain sizes necessary for the required absorption and compare them with the expected scale. Systems that predict grains far too small to be realistic are essentially unaffected by absorption. This method for estimating plausibility is approximate, and detailed modeling is required to determine the exact drop in intensity that would be caused by this granular material along the line of sight. Our model assumes monodisperse grains, but in reality the grain radius is given by a distribution over sizes. For all but two ESE observations given in Table 1, the predicted grain radii appear plausible for the observed lens parameters on the order of both 1% and 5% adjustment of the magnified image intensity. In principle, this suggests plausible absorption may be compatible with current observations and models, depending on the uncertainty in the fits. The observations correspond to ESEs in the systems 1741+038, 2023+335, PKS 1939-315, PSR B1937+21, PSR J1603-7202, and PSR J1017-7156. If absorption is important in these lens structures, perhaps some evidence of their existence could be revealed through multi-band observations, probing the lens at many frequencies as the ESE is ongoing. The wavelength evolution of the models separates cold plasma from absorbing Drude material, which is fixed by observation. We do not suggest the observed ESEs are Drude lenses due to the observed wavelength behavior. However, our study does show that, in principle, absorbing material within ESE scale lenses is plausible at observable scales and that achromatic ESE-like events would provide evidence toward the existence of such dusty, absorbing lenses.

Dust grains in the ISM obey a power-law [56], and there is uncertainty in both ends of the size range, such that 0.1 nm grains may be physically plausible. Only one of the eleven observations predicts grain sizes that are unphysically small. The system PSR B1800-21 is strictly incompatible with observations, predicting grain size that potentially ranges between ∼0.001–0.005 nm, which is more than two orders of magnitude outside the 0.1 nm range. The system 0954+658 is on the edge of this limit at both 1% and 5% intensity, with a predicted grain size between 0.078–0.399 nm.

Given that the majority of ESEs considered in Table 1 could support absorbing material with a slight modification to observed models, we conclude tentatively that absorption due to dielectric dust or other materials within the lenses responsible for ESEs is plausible; however, further study with a more realistic model in which the dust density varies are required.

Additionally, we studied the thin-lens formalism to describe the geometry necessary for the formation of X-ray haloes by dust scattering. In this limit, the model predicts only weak lensing effects (equivalent to low-angle scattering).

Funding: This research received no external funding.

Data Availability Statement: No new data were created in this study.

Acknowledgments: This work is dedicated to Jason D. Fiege, Samar Safi-Harb, and Kurt Hildebrand of the University of Manitoba, Department of Physics & Astronomy. Your many contributions to my career are appreciated beyond words can express.

Conflicts of Interest: The author declares no conflicts of interest.

Abbreviations

The following abbreviations are used in this manuscript:

GRB	Gamma-ray burst
FRB	Fast radio burst
ISM	Interstellar medium
ESE	Extreme scattering event
CFL	Clegg, Fey, Lazio

References

1. Bisnovatyi-Kogan, G.S.; Tsupko, O.Y. Gravitational Lensing in Presence of Plasma: Strong Lens Systems, Black Hole Lensing and Shadow. *Universe* **2017**, *3*, 57. [CrossRef]
2. Schneider, P.; Ehlers, J.; Falco, E.E. *Gravitational Lenses, XIV*; Springer: Berlin/Heidelberg, Germany; New York, NY, USA, 1992.
3. Narayan, R.; Bartelmann, M. Lectures on Gravitational Lensing. *arXiv* **1996**, arXiv:9606001.
4. Belokurov, V.; Evans, N.W.; Moiseev, A.; King, L.J.; Hewett, P.C.; Pettini, M.; Wyrzykowski, L.; McMahon, R.G.; Smith, M.C.; Gilmore, G.; et al. The cosmic horseshoe: Discovery of an einstein ring around a giant luminous red galaxy. *Astrophys. J.* **2007**, *671*, L9–L12. [CrossRef]
5. Clegg, A.W.; Fey, A.L.; Lazio, T.J.W. The Gaussian plasma lens in astrophysics: Refraction. *Astrophys. J.* **1998**, *496*, 253–266. [CrossRef]
6. Stanimirović, S.; Zweibel, E.G. Atomic and Ionized microstructures in the diffuse interstellar medium. *Ann. Rev. Astron. Astrophys.* **2018**, *56*, 489–540. [CrossRef]
7. Perlick, V. *Ray Optics, Fermat's Principle and Applications to General Relativity*; Springer: Berlin/Heidelberg, Germany, 2000.
8. Rogers, A. Frequency-dependent effects of gravitational lensing within plasma. *Mon. Not. R. Astron. Soc.* **2015**, *451*, 17–25. [CrossRef]
9. Klose, S. X-ray halos and the size distribution of the cosmic grains. *Astron. Astrophys.* **1991**, *248*, 624–632.
10. Mauche, C.W.; Gorenstein, P. Measurements of X-ray scattering from interstellar grains. *Astrophys. J.* **1986**, *302*, 371–387. [CrossRef]
11. Hayakawa, S. Scattering of cosmic X-rays by interstellar dust grains. *Prog. Theor. Phys.* **1970**, *43*, 5. [CrossRef]
12. Evans, A.; Norwell, G.A.; Bode, M.F. X-ray scattering by intergalactic dust. *Mon. Not. R. Astron. Soc.* **1985**, *1985*, 213.
13. Lamer, G.; Schwope, A.D.; Predehl, P.; Traulsen, I.; Wilms, J.; Freyberg, M. A giant X-ray dust scattering ring discovered with SRG/eROSITA around the black hole transient MAXI J1348–630. *Astron. Astrophys.* **2021**, *647*, A7. [CrossRef]
14. Tiengo, A.; Vianello, G.; Esposito, P.; Mereghetti, S.; Giuliani, A.; Costantini, E.; Israel, G.L.; Stella, L.; Turolla, R.; Zane, S.; et al. The dust-scattering X-ray rings of the anomalous X-ray pulsar 1E 1547.0–5408. *Astrophys. J.* **2010**, *710*, 227. [CrossRef]
15. Heinz, S.; Burton, M.; Braiding, C.; Brandt, W.N.; Jonker, P.G.; Sell, P.; Fender, R.P.; Nowak, M.A.; Schulz, N.S. Lord of the rings: A kinematic distance to Circinus X-1 from a giant X-ray light echo. *Astrophys. J.* **2015**, *806*, 265. [CrossRef]
16. Barthelmy, S.D.; D'Ai, A.; D'Avanzo, P.; Krimm, H.A.; Lien, A.Y.; Marshall, F.E.; Maselli, A.; Siegel, M.H. GCN Circulars 17929. 2015. Available online: https://gcn.nasa.gov/circulars/17929 (accessed on 19 January 2025).
17. Rodriguez, J.; Cadolle Bel, M.; Alfonso-Garzón, J.; Siegert, T.; Zhang, X.-L.; Grinberg, V.; Savchenko, V.; Tomsick, J.A.; Chenevez, J.; Clavel, M.; et al. Correlated optical, X-ray, and γ-ray flaring activity seen with INTEGRAL during the 2015 outburst of V404 Cygni. *A&A* **2015**, *581*, L9.
18. Tiengo, A.; Pintore, F.; Vaia, B.; Filippi, S.; Sacchi, A.; Esposito, P.; Rigoselli, M.; Mereghetti, S.; Salvaterra, R.; Šiljeg, B.; et al. The power of the rings: The GRB 221009A soft X-ray emission from its dust-scattering halo. *Astrophys. J. Lett.* **2023**, *946*, L30. [CrossRef]
19. Corrales, L.; Mills, B.S.; Heinz, S.; Williger, G.M. The X-ray variable sky as seen by MAXI: The future of dust-echo tomography with bright galactic X-ray bursts. *Astrophys. J.* **2019**, *874*, 155. [CrossRef]
20. Lorimer, D.R.; McLaughlin, M.A.; Bailes, M. The discovery and significance of fast radio bursts. *Astrop. Space Sci.* **2024**, *369*, 59. [CrossRef]
21. Wagner, J.; Er, X. Plasma lensing in comparison to gravitational lensing–Formalism and degeneracies. *arXiv* **2020**, arXiv:2006.16263.
22. Rogers, A. Ray tracing through absorbing dielectric media in the Schwarzschild spacetime. *Class. Quant. Grav.* **2024**, *41*, 175007. [CrossRef]
23. Ashcroft, N.; Mermin, N.D. *Solid State Physics*; Holt, Rinehart and Winston: New York, NY, USA, 1976.
24. Esteban, J.M.; Orazem, M.E. On the application of the kramers-kronig relations to evaluate the consistency of electrochemical impedance data. *J. Electrochem. Soc.* **1991**, *138*, 67. [CrossRef]

25. Agarwal, P.; Orazem, M.E.; Garcia-Rubio, L.H. Measurement models for electrochemical impedance spectroscopy: I Demonstration of applicability. *J. Electrochem. Soc.* **1992**, *139*, 1917. [CrossRef]
26. Boukamp, B.A. A linear Kronig-Kramers transform test for immittance data validation. *J. Electrochem. Soc.* **1995**, *142*, 1885–1894. [CrossRef]
27. Dressel, M.; Gruner, G. *Electrodynamics of Solids: Optical Properties of Electrons in Matter*; Cambridge University Press: New York, NY, USA, 2003.
28. Breuer, R.A.; Ehlers, J. Propagation of high-frequency electromagnetic waves through a magnetized plasma in curved space-time. I. *Proc. R. Soc. Lond. A* **1980**, *370*, 389–406.
29. Breuer, R.A.; Ehlers, J. Propagation of electromagnetic waves through magnetized plasmas in arbitrary gravitational fields. *Astron. Astrophys.* **1981**, *96*, 293–295.
30. Noonan, T.W. Light rays in gravitating, refractive media. *Astrophys. J.* **1982**, *262*, 344–348. [CrossRef]
31. Smith, R.K.; Dwek, E. Soft X-ray scattering and halos from dust. *Astrophys. J.* **1998**, *503*, 831–842. [CrossRef]
32. Corrales, L.R.; Garcia, J.; Wilms, J.; Baganoff, F. The dust-scattering component of X-ray extinction: Effects on continuum fitting and high-resolution absorption edge structure. *Mon. Not. R. Astron. Soc.* **2016**, *458*, 1345–1351. [CrossRef]
33. Tuntsov, A.V.; Walker, M.A.; Koopmans, L.V.; Bannister, K.W.; Stevens, J.; Johnston, S.; Reynolds, C.; Bignall, H.E. Dynamic spectral mapping of interstellar plasma lenses. *Astrophys. J.* **2016**, *817*, 176. [CrossRef]
34. Bisnovatyi-Kogan, G.S.; Tsupko, O.Y. Gravitational radiospectrometer. *Grav. Cosmol.* **2009**, *15*, 20–27. [CrossRef]
35. Gradshtein, I.S.; Ryzhik, I.M. *Tables of Integrals, Series and Products*, 7th ed.; Academic Press: Burlington, MA, USA, 2007.
36. Drude, P. Zur elektronentheorie der metalle. *Ann. Phys.* **1900**, *306*, 566–613. [CrossRef]
37. Cordes, J.M. Lensing of fast radio bursts by plasma structures in host galaxies. *Astrophys. J.* **2017**, *842*, 1. [CrossRef]
38. Er, X.; Yang, Y.-P.; Rogers, A. The effects of plasma lensing on the inferred dispersion measures of fast radiobursts. *Astrophys. J.* **2020**, *889*, 158. [CrossRef]
39. Li, A. Optical properties of dust. *arXiv* **2008**, arXiv:0808.4123.
40. Predehl, P.; Schmitt, J.H.M.M. X-raying the interstellar medium: ROSAT observations of dust scattering halos. *Astron. Astrophys.* **1995**, *293*, 889–905.
41. Vedantham, H.K.; Readhead, A.C.; Hovatta, T.; Koopmans, L.V.; Pearson, T.J.; Blatford, R.D.; Gurwell, M.A.; Lähteenmäki, A.; Max-Moerbeck, W.; Pavlidou, V.; et al. The peculiar light curve of J1415+ 1320: A case study in extreme scattering events. *Astrophys. J.* **2017**, *845*, 90. [CrossRef]
42. Pushkarev, A.B.; Kovalev, Y.Y.; Lister, M.L.; Hovatta, T.; Savolainen, T.; Aller, M.F.; Aller, H.D.; Ros, E.; Zensus, J.A.; Richards, J.L.; et al. VLBA observations of a rare multiple quasar imaging event caused by refraction in the interstellar medium. *Astron. Astrophys.* **2013**, *555*, A80. [CrossRef]
43. Bannister, K.W.; Stevens, J.; Tuntsov, A.V.; Walker, M.A.; Johnston, S.; Reynolds, C.; Bignall, H. Real-time detection of an extreme scattering event: Constraints on Galactic plasma lenses. *Science* **2016**, *351*, 354–356. [CrossRef]
44. Maitia, V.; Lestrade, J.F.; Cognard, I. A 3 year long extreme scattering event in the direction of the millisecond pulsar J1643–1224. *Astrophys. J.* **2003**, *582*, 972–977. [CrossRef]
45. Cognard, I.; Bourgois, G.; Lestrade, J.F.; Biraud, F.; Aubry, D.; Darchy, B.; Drouhin, J.P. An extreme scattering event in the direction of the millisecond pulsar 1937+ 21. *Nature* **1993**, *366*, 320–322. [CrossRef]
46. Lestrade, J.-F.; Rickett, B.J.; Cognard, I. Interstellar modulation of the flux density and arrival time of pulses from pulsar B 1937+ 214. *Astron. Astrophys.* **1998**, *334*, 1068–1084.
47. Basu, R.; Rozko, K.; Lewandowski, W.; Kijak, J.; Dembska, M. Time variation in the low-frequency spectrum of Vela-like pulsar B1800–21. *Mon. Not. R. Astron. Soc.* **2016**, *458*, 2509–2515. [CrossRef]
48. Coles, W.A.; Kerr, M.; Shannon, R.M.; Hobbs, G.B.; Manchester, R.N.; You, X.P.; Bailes, M.; Bhat, N.D.; Burke-Spolaor, S.; Dai, S.; et al. Pulsar observations of extreme scattering events. *Astrophys. J.* **2015**, *808*, 113. [CrossRef]
49. Er, X.; Rogers, A. Two families of astrophysical diverging lens models. *Mon. Not. R. Astron. Soc.* **2018**, *475*, 867–878. [CrossRef]
50. Trumper, J.; Schonfelder, V. Distance determination of variable X-ray sources. *Astron. Astrophys.* **1973**, *25*, 445.
51. Predehl, P.; Burwitz, V.; Paerels, F.; Trümper, J. Chandra measurement of the geometrical distance to Cyg X-3 using its X-ray scattering halo. *Astron. Astrophys.* **2000**, *357*, L25–L28.
52. Predehl, P.; Klose, S. Dust scattered X-ray haloes as diagnostic tools: Potential and current limitations. *Astron. Astrophys.* **1995**, *306*, 283–293.
53. Miralda-Escude, J. Small-angle scattering of x-rays from extragalactic sources by dust in intervening galaxies. *Astrophys. J.* **1999**, *512*, 21–24. [CrossRef]
54. Refsdal, S. On the possibility of testing cosmological theories from the gravitational lens effect. *Mon. Not. R. Astron. Soc.* **1966**, *132*, 101. [CrossRef]

55. Pen, U.-L.; King, L. Refractive convergent plasma lenses explain extreme scattering events and pulsar scintillation. *Mon. Not. R. Astron. Soc. Lett.* **2012**, *421*, L132–L136. [CrossRef]
56. Mathis, J.S.; Rumpl, W.; Nordsieck, K.H. The size distribution of interstellar grains. *Astrophys. J.* **1977**, *217*, 425. [CrossRef]